International Journal of Modern Physics A
© World Scientific Publishing Company

arXiv:2204.13315v1 [quant-ph] 28 Apr 2022

The Casimir effect in graphene systems: Experiment and theory

G. L. Klimchitskaya,[1,2] U. Mohideen[3] and V. M. Mostepanenko[1,2,4]

[1] *Central Astronomical Observatory at Pulkovo of the Russian Academy of Sciences, Saint Petersburg, 196140, Russia*
[2] *Peter the Great Saint Petersburg Polytechnic University, Saint Petersburg, 195251, Russia*
[3] *Department of Physics and Astronomy, University of California, Riverside, California 92521, USA*
[4] *Kazan Federal University, Kazan, 420008, Russia*
g_klimchitskaya@mail.ru, Umar.Mohideen@ucr.edu, vmostepa@gmail.com

Received Day Month Year
Revised Day Month Year

The Casimir effect in graphene systems is reviewed with emphasis made on the large thermal correction to the Casimir force predicted at short separations between the test bodies. The computational results for the Casimir pressure and for the thermal correction are presented for both pristine graphene and real graphene sheets, which possess nonzero energy gap and chemical potential, obtained by means of exact polarization tensor. Two experiments on measuring the gradient of the Casimir force between an Au-coated sphere and graphene- coated substrates performed by using a modified atomic force microscope cantilever-based technique are described. It is shown that the measurement data of both experiments are in agreement with theoretical predictions of the Lifshitz theory using the polarization tensor. Additionally, several important improvements made in the second experiment, allowed to demonstrate the predicted large thermal effect in the Casimir interaction at short separations. Possible implications of this result to resolution of long-term problems of Casimir physics are discussed.

Keywords: Casimir force; graphene; Lifshitz theory; polarization tensor; precise measurements; atomic force microscope; thermal correction.

PACS Nos.: 68.65.Pq; 12.20.Fv; 12.20.Ds; 12.20.-m

1. Introduction

The Casimir effect[1] is an extraordinary physical phenomenon which has been much investigated in several fields of physics for almost 75 years after its discovery. According to Casimir's result, two parallel ideal metal planes in vacuum attract each other by a force which depends only on the Planck constant $\hbar$, speed of light c, and the separation between the planes. This force originates from the zero-point fluctuations of the quantum electromagnetic field. If the planes are at temperature T in thermal equilibrium with the environment, the force value is also determined by the value of T and the Boltzmann constant k_B. The thermal Casimir force is caused by the joint action of the zero-point and thermal fluctuations.

Lifshitz[2,3] developed a general theory of the Casimir force between two material plates described by the frequency-dependent dielectric permittivities. In the last 20 years this theory has been shown to have problems when comparing theoretical predictions with the measurement data of high precision experiments and with the requirements of thermodynamics (see an extensive review[4–7] and the most recent experiments[8–11]). One conceivable reason for these problems is that the dielectric permittivities describing the response of the plate materials to electromagnetic fluctuations are to a large measure of phenomenological character and may fail to account for all subtle features of the field-matter interaction.

In this regard graphene, which is a 2D sheet of carbon atoms packed in a hexagonal lattice[12–16] is of immediate interest to theorists and experimentalists working in the Casimir effect. The reason is that at energies below some definite value (which was estimated[17] as approximately equal to 3 eV) graphene is well described in the framework of the Dirac model as a set of either massless or very light electronic quasiparticles. The quantum field of these quasiparticles satisfies the relativistic Dirac equation in 2+1 dimensions[12–16] with the only difference that the speed of light is replaced with the Fermi velocity $v_{\rm F} \approx c/300$.

Given that graphene is so simple a physical system, it becomes possible to find its dielectric response to electromagnetic fluctuations starting from the first principles of quantum electrodynamics at nonzero temperature without resorting to phenomenological methods. This was done by finding the polarization tensor of graphene[18–21] which is equivalent to two spatially nonlocal dielectric permittivities, the longitudinal one and the transverse one, depending on both the frequency and the wave vector.[22] In so doing the Casimir interaction between two graphene sheets is described by the standard Lifshitz formulas where the reflection coefficients take the non-Fresnel form and are expressed via the components of the polarization tensor. This offers strong possibilities of reliable theoretical predictions for the Casimir interaction between two graphene sheets and graphene-coated substrates which can be tested experimentally and checked for a consistency with the requirements of thermodynamics.

The first experiment on measuring the gradient of the Casimir force between an Au-coated sphere and a graphene sheet on a Si-SiO_2 substrate was performed by means of an atomic force microscope (AFM) operated in the frequency shift technique.[23] The measurement results were found to be in good agreement with theoretical predictions by using the polarization tensor.[24] Due to the small thickness of the SiO_2 substrate,[25] it was, however, not possible to detect the large thermal effect in the Casimir force at short separations predicted previously for graphene.[26]

In the second experiment on measuring the gradient of the Casimir force from graphene by means of an AFM, a thicker SiO_2 substrate was used. In addition, the energy gap Δ caused by a nonzero mass of quasiparticles and the chemical potential μ caused by the presence of impurities in the graphene sample have been found utilizing scanning tunneling spectroscopy and Raman spectroscopy, respectively.[27,28]

The measurement data were compared with theoretical predictions using the polarization tensor and the existence of large thermal effect was confirmed over the range of separations from 250 to 517 nm.

In this review, we consider all the above results with due regard to the investigation of the Casimir effect in graphene systems performed using some other techniques. In Sec. 2, the Lifshitz formulas describing the Casimir interaction between two graphene sheets and between graphene-coated substrates using the formalism of the polarization tensor are presented. Section 3 is devoted to the thermal Casimir force from the sheets of pristine and real graphene. In Sec. 4, the first experiment on measuring the gradient of the Casimir force from graphene is described. Demonstration of the unusual thermal effect in the Casimir interaction from graphene made in the second experiment is contained in Sec. 5. Finally, in Sec. 6, the reader will find our conclusions and discussion of the obtained results for the Casimir force from graphene with their possible implication to other materials.

2. Lifshitz Formula, Electromagnetic Response of Graphene, and the Polarization Tensor

According to the scattering theory approach to electrodynamic Casimir forces,[29–31] the standard Lifshitz formulas for the Casimir free energy per unit area $\mathcal{F}$ and pressure P, originally derived[2] for the case of two semispaces, remain valid for any two planar structures with appropriately defined reflection coefficients $R_{\rm TM}^{(n)}$ and $R_{\rm TE}^{(n)}$, $n = 1, 2$, for the transverse magnetic and transverse electric polarizations of the electromagnetic field. They are as follows:

$$\mathcal{F}(a,T) = \frac{k_B T}{2\pi}{\sum_{l=0}^{\infty}}' \int_0^{\infty} k_\perp dk_\perp \sum_\lambda \ln\left[1 - R_\lambda^{(1)}(i\xi_l, k_\perp) R_\lambda^{(2)}(i\xi_l, k_\perp) e^{-2aq_l}\right] \quad (1)$$

and

$$P(a,T) = -\frac{k_B T}{\pi}{\sum_{l=0}^{\infty}}' \int_0^{\infty} q_l k_\perp dk_\perp \sum_\lambda \left[\frac{e^{2aq_l}}{R_\lambda^{(1)}(i\xi_l, k_\perp) R_\lambda^{(2)}(i\xi_l, k_\perp)} - 1\right]^{-1}. \quad (2)$$

Here, a is a separation between the plane structures, the prime on the summation in l divides the term with $l = 0$ by 2, $k_\perp$ is the magnitude of the wave vector projection on the planar structures, $\xi_l = 2\pi k_B T l/\hbar$ are the Matsubara frequencies, $q_l = (k_\perp^2 + \xi_l^2/c^2)^{1/2}$, and $\lambda = (\text{TM, TE})$. The quantities $R_\lambda^{(n)}$ may have a meaning of the reflection coefficients on metallic or dielectric plates, on graphene sheets or on the graphene-coated substrates.

There are many theoretical approaches to calculation of the reflection coefficients on a graphene sheet based on a hydrodynamic model,[32–34] Kubo theory,[35–37] density-density correlation functions found in the random phase approximation,[26,38–42] in-plane and out-of-plane electrical conductivities of graphene obtained by means of the 2D Drude model, Kubo formula etc.[37,40,42–46] It should be

noted, however, that the exact expressions for the correlation functions and conductivities of graphene at any nonzero temperature remained unknown. Specifically, the conductivities calculated using the Kubo formula include the phenomenological relaxation parameter and neglect the energy gap of graphene.

As mentioned in Sec. 1, at energies below 3 eV the Dirac model provides a comprehensive fundamental description of graphene (note that the first absorption peak of graphene takes place at larger energy of $\hbar\omega \approx 4.59$ eV). Taking into account that measurements of the Casimir interaction by means of the dynamic AFM are performed at separations exceeding 200 nm, which correspond to the characteristic energies $\hbar c/(2a) < 0.5$ eV, an application of the Dirac model for calculation of the Casimir force from graphene is fully justified.

In the framework of the Dirac model, the reflection coefficients on a graphene sheet can be expressed via its polarization tensor $\Pi_{\beta\gamma,l} = \Pi_{\beta\gamma}(i\xi_l, k_\perp, T, \Delta, \mu)$ found using the formalism of quantum electrodynamics at nonzero temperature.[18–21] For real graphene sheets the components of the polarization tensor ($\beta, \gamma = 0, 1, 2$) depend on the energy gap $\Delta = 2mv_{\rm F}^2$, where m is the mass of quasiparticles, and on the chemical potential μ. For generality, we present the reflection coefficients on thick material plates with the dielectric permittivities $\varepsilon_l^{(n)} = \varepsilon^{(n)}(i\xi_l)$ coated with a graphene sheet[24,47,48]

$$R_{\rm TM}^{(n)}(i\xi_l, k_\perp) = \frac{\hbar k_\perp^2[\varepsilon_l^{(n)} q_l - k_l^{(n)}] + q_l k_l^{(n)} \Pi_{00,l}}{\hbar k_\perp^2[\varepsilon_l^{(n)} q_l + k_l^{(n)}] + q_l k_l^{(n)} \Pi_{00,l}},$$
$$R_{\rm TE}^{(n)}(i\xi_l, k_\perp) = \frac{\hbar k_\perp^2[q_l - k_l^{(n)}] - \Pi_l}{\hbar k_\perp^2[q_l + k_l^{(n)}] + \Pi_l}, \tag{3}$$

where $k_l^{(n)} = [k_\perp^2 + \varepsilon_l^{(n)} \xi_l^2/c^2]^{1/2}$ and the quantity Π_l is expressed via the trace of the polarization tensor and its 00-component according to:

$$\Pi_l = k_\perp^2 \Pi_{\beta,l}^{\beta} - q_l^2 \Pi_{00,l}. \tag{4}$$

The reflection coefficients on the freestanding (with no substrate) graphene sheet are obtained from (3) by putting $\varepsilon_l^{(n)} = 1$, $k_l^{(n)} = q_l$. The standard (Fresnel) reflection coefficients on the plates made of ordinary materials are obtained from (3) by putting $\Pi_{00,l} = \Pi_l = 0$.

It is convenient to present the quantities $\Pi_{00,l}$ and Π_l in the form

$$\Pi_{00,l} = \Pi_{00,l}^{(0)} + \Pi_{00,l}^{(1)}, \quad \Pi_l = \Pi_l^{(0)} + \Pi_l^{(1)}, \tag{5}$$

where $\Pi_{00,l}^{(0)}$ and $\Pi_l^{(0)}$ refer to the polarization tensor of graphene with perfect hexagonal lattice with no impurities ($\mu = 0$), zero temperature ($T = 0$), and any value of the energy gap Δ. By construction, the terms $\Pi_{00,l}^{(0)}$ and $\Pi_l^{(0)}$ in (5) do not depend on T as a parameter but only implicitly, through the Matsubara frequencies, as they are calculated at $\omega = i\xi_l$. By contrast, the terms $\Pi_{00,l}^{(1)}$ and $\Pi_l^{(1)}$ in (5) include an explicit dependence of the polarization tensor on T as a parameter. They also depend on the chemical potential μ and the energy gap Δ.

The terms $\Pi^{(0)}_{00,l}$ and $\Pi^{(0)}_{l}$ are given by[18,19]

$$\Pi^{(0)}_{00,l}=\frac{\alpha\hbar k_\perp^2}{\tilde{q}_l}\Psi(D_l), \quad \Pi^{(0)}_{l}=\alpha\hbar k_\perp^2\tilde{q}_l\Psi(D_l), \tag{6}$$

where $\alpha=e^2/(\hbar c)$ is the fine structure constant and the following notations are introduced

$$\Psi(x)=2\left[x+(1-x^2)\arctan\frac{1}{x}\right], \quad \tilde{q}_l=\sqrt{\frac{v_F^2}{c^2}k_\perp^2+\frac{\xi_l^2}{c^2}}, \quad D_l=\frac{\Delta}{\hbar c\tilde{q}_l}. \tag{7}$$

The second terms on the right-hand side of (5) take the form[21,48]

$$\begin{aligned}
\Pi^{(1)}_{00,l}&=\frac{4\alpha\hbar c^2\tilde{q}_l}{v_F^2}\int_{D_l}^{\infty}du\left(\sum_{\kappa=\pm1}\frac{1}{e^{B_lu+\kappa\frac{\mu}{k_BT}}+1}\right)\\
&\times\left[1-\mathrm{Re}\frac{1-u^2+2i\gamma_lu}{\left(1-u^2+2i\gamma_lu+D_l^2-\gamma_l^2D_l^2\right)^{1/2}}\right],\\
\Pi^{(1)}_{l}&=-\frac{4\alpha\hbar\tilde{q}_l\xi_l^2}{v_F^2}\int_{D_l}^{\infty}du\left(\sum_{\kappa=\pm1}\frac{1}{e^{B_lu+\kappa\frac{\mu}{k_BT}}+1}\right)\\
&\times\left[1-\mathrm{Re}\frac{(1+i\gamma_l^{-1}u)^2+(\gamma_l^{-2}-1)D_l^2}{\left(1-u^2+2i\gamma_lu+D_l^2-\gamma_l^2D_l^2\right)^{1/2}}\right],
\end{aligned} \tag{8}$$

where $\gamma_l\equiv\xi_l/(c\tilde{q}_l)$ and $B_l\equiv\hbar c\tilde{q}_l/(2k_BT)$.

Note that the density-density correlation functions and the spatially nonlocal dielectric permittivities of graphene are uniquely determined by its polarization tensor.[49] For instance, the transverse and longitudinal permittivities are given by

$$\varepsilon_l^{\mathrm{Tr}}=1+\frac{c^2}{2\hbar k_\perp\xi_l^2}\Pi_l \qquad \varepsilon_l^{\mathrm{L}}=1+\frac{1}{2\hbar k_\perp}\Pi_{00,l}. \tag{9}$$

Thus, the exact expressions (5)–(8) for the polarization tensor also provide the respective expressions for the density-density correlation functions of graphene at any temperature and make both formalisms equivalent.[49]

Using the Casimir free energy $\mathcal{F}$ (1) with the reflection coefficients (3)–(8), one can define the Casimir entropy

$$S(a,T)=-\frac{\partial\mathcal{F}(a,T)}{\partial T} \tag{10}$$

and determine its behavior with vanishing temperature. For two pristine graphene sheets ($\varepsilon_l^{(n)}=1$, $\Delta=\mu=0$) it was shown[50] that the Casimir entropy goes to zero when the temperature vanishes in line with the Nernst heat theorem. The same was proven[51] for two real graphene sheets characterized by nonzero values of the energy gap and chemical potential. Similar results were obtained[52,53] for the Casimir-Polder entropy related to an atom interacting with a graphene sheet (see also the review in Ref. 54).

One can conclude that the Lifshitz theory of the Casimir interaction between graphene sheets is in perfect agreement with the requirements of thermodynamics if the dielectric response of graphene is described by the formalism of the polarization tensor.

3. Thermal Casimir Force from Sheets of Pristine and Real Graphene

The formalism of Sec. 2 allows calculation of the thermal Casimir force between pristine and real graphene sheets as well as between different material plates and a graphene sheet either freestanding or deposited on a substrate. Below we present several characteristic results of this kind which give an idea of the thermal effect in the Casimir force from graphene as opposed to ordinary materials.

We start with the simplest configuration of two parallel sheets of pristine graphene at room temperature $T = 300$ K. The thermal Casimir pressure in this configuration is computed[47] by (2) and (3)–(8) where one should put $\varepsilon_l^{(n)} = 1$ and $\Delta = \mu = 0$. In Fig. 1 (left), the computational results for the magnitude of the Casimir pressure $|P|$ normalized to the quantity $B = k_B T/(8\pi a^3)$ are shown as a function of separation by the top line.

To gain a better understanding of the role of thermal effects, we consider separately the impact of the explicit and implicit thermal dependence on the Casimir pressure. For this purpose, we repeat the same computations as above, but with only the first term of the polarization tensor in (5) given by (6). This term does not include the explicit dependence of the polarization tensor on T as a parameter and depends on temperature only implicitly through the Matsubara frequencies. The obtained computational results for $|P|/B$, as a function of separation, are shown by

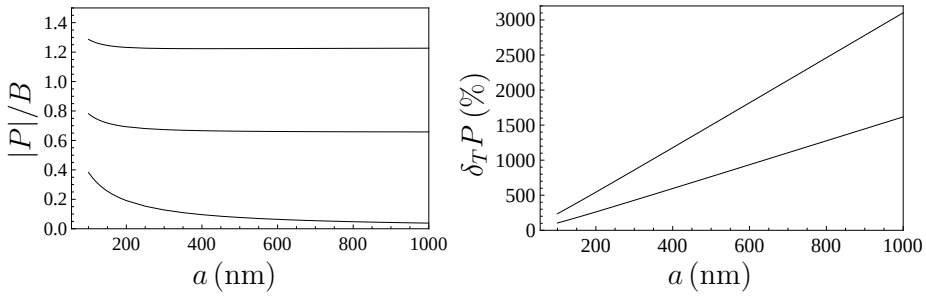


Fig. 1. The normalized magnitudes of the Casimir pressure between two pristine freestanding graphene sheets are shown as functions of separation. The top and middle lines are computed at $T = 300$ K using the full polarization tensor and its zero-temperature contribution taken at the Matsubara frequencies, respectively. The bottom line is computed at $T = 0$ K (left). The relative thermal corrections to the Casimir pressure between two pristine freestanding graphene sheets are shown as functions of separation by the top and bottom lines computed at $T = 300$ K using the full polarization tensor and its zero-temperature contribution taken at the Matsubara frequencies, respectively (right).

the middle line in Fig. 1 (left).

Next, the bottom line in Fig. 1 (left) is computed by the same formulas as the middle line, but at $T = 0$ K in the strict sense. This means that the summation over the Matsubara frequencies in (1) is replaced with an integration in continuous frequency according to

$$k_B T \sum_{l=0}^{\infty}{}' \to \frac{\hbar}{2\pi} \int_0^\infty d\xi. \tag{11}$$

Thus, a difference between the middle and bottom lines in Fig. 1 (left) illustrates the role of an implicit thermal effect in the Casimir pressure between two graphene sheets whereas a difference between the top and middle lines shows the contribution from an explicit dependence of the polarization tensor on temperature as a parameter. As is seen in Fig. 1 (left), in the region of separations considered, both thermal effects contribute to the Casimir pressure roughly equally.

The role of thermal effects in the Casimir pressure between the sheets of pristine graphene can be expressed quantitatively by the relative thermal correction

$$\delta_T P(a,T) = \frac{\Delta_T P(a,T)}{P(a,0)} = \frac{P(a,T) - P(a,0)}{P(a,0)}. \tag{12}$$

In Fig. 1 (right), the computational results for $\delta_T P$ at $T = 300$ K are presented as functions of separation by the top and bottom lines computed with the full polarization tensor (5), (6), (8) and the polarization tensor (6) defined at $T = 0$, respectively. Thus, the top line presents the total thermal effect whereas the bottom line — only the implicit one. In fact both these effects are unexpectedly large. For example, at 100, 200, 600, and 1000 nm the total thermal correction constitutes 236%, 544%, 1818%, and 3101% of the zero-temperature Casimir pressure, respectively. The implicit thermal correction constitutes 104%, 262%, 935%, and 1617% at the same respective separations.

An unusually large thermal effect in the Casimir pressure between two graphene sheets at short separations was first predicted[26] by using the method of density-density correlation functions in the random phase approximation. It can be considered as unusual because for ordinary materials at separations below a micrometer the thermal effect does not exceed a fraction of a percent (a few percent effect predicted for metals when using an extrapolation of the optical data by means of the Drude model was experimentally excluded[4–11]). So the large magnitude of the thermal effect for graphene can be explained physically[26,28] by the fact that, in addition to the standard effective temperature $k_B T_{\rm eff} = \hbar c/(2a)$ inherent to all materials, graphene is also characterized by much lower effective temperature $k_B \tilde{T}_{\rm eff} = \hbar v_{\rm F}/(2a)$.

The computational results obtained using different theoretical approaches to the Casimir force in graphene systems listed in Sec. 2 were correlated with the results found by means of the polarization tensor.[55] This was helpful in the determination of the regions of applicability of each approach and in the justification of the results

using various phenomenological models. Specifically, it was shown that for a pristine graphene the calculation approaches, which neglect the temperature dependence of its dielectric response, could be applicable only at the shortest separations of about a few angströms. At the same time, the computational results using the polarization tensor are in agreement[55] with nonrelativistic computations using Coulomb coupling between density fluctuations with subsequent thermal averaging employed in the first publication which predicted the unusual thermal effect in the Casimir force from graphene.[26]

Now we consider the impact of the nonzero gap and chemical potential on the size of thermal correction to the Casimir pressure. Note that a nonzero energy gap and chemical potential are inevitable with real graphene sheets particularly those on substrates as used in experiments.[23,27,28] As in experiments on measuring the Casimir force from graphene one body is metallic, we consider an Au plate interacting with the freestanding either pristine or real graphene sheet with $\Delta = 0.29$ eV and $\mu = 0.24$ eV (these are the experimental parameters, see Sec. 5). Computations of the thermal correction in each case are again performed by (2), (3)–(8) and (12). In both cases one should put $\Pi_{00,l} = \Pi_l = 0$ in the reflection coefficients $R_\lambda^{(1)}$ from (3) and substitute $\varepsilon_l^{(1)}$ for Au obtained from the optical data[56] extrapolated down to zero frequency[2,4] (the type of extrapolation does not influence the obtained results in this case due to a smallness of the TE reflection coefficient for graphene at zero frequency). As to the coefficients $R_\lambda^{(2)}$, one should put $\varepsilon_l^{(2)} = 1$ and use $\Delta = \mu = 0$ for a pristine graphene sheet and the specific values indicated above for a real one.

The computational results for the relative thermal correction to the Casimir pressure between an Au plate and either pristine or real graphene sheet are shown as the functions of separation in Fig. 2 (left) by the top and bottom pairs of lines,

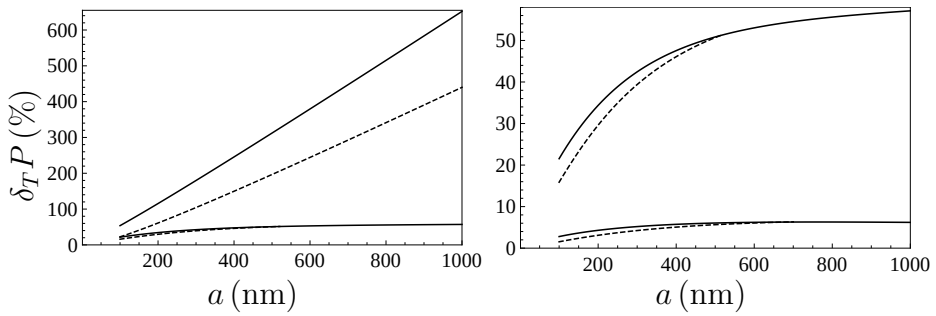


Fig. 2. The relative thermal corrections to the Casimir pressure between an Au plate and either pristine or real freestanding graphene sheets are shown as functions of separation by the top and bottom pairs of lines, respectively (left). The relative thermal corrections to the Casimir pressure between an Au plate and a real graphene sheet deposited on a SiO_2 plate are shown by the bottom pair of lines (right). In each pair, the solid line is computed at $T = 300$ K using the full polarization tensor and the dashed line — its zero-temperature contribution taken at the Matsubara frequencies. The top pair of lines (right) reproduces the bottom pair of lines (left).

respectively. In each pair, the solid line indicates the total thermal correction and the dashed line presents the implicit thermal correction with neglected explicit dependence of polarization tensor on temperature as a parameter. In this case the thermal effect originates entirely from a summation over the Matsubara frequencies.

As is seen from the top solid line in Fig. 2 (left), for an Au plate interacting with a pristine graphene sheet the thermal correction, though large enough, is much smaller than for two pristine graphene sheets. At $a = 100$, 200, 600, and 1000 nm, it constitutes 53.7%, 115.5%, 379.5%, and 659.9% of the Casimir pressure calculated at $T = 0$, respectively. These should be compared with the respective values related to the top line in Fig. 1 (right) which are by almost a factor of 5 larger. From the top dashed line in Fig. 2 (left), one finds that at the same respective separations the implicit thermal correction constitutes 22.5%, 61.1%, 244.2% and 439.9%. Thus, in this case, the role of implicit correction increases with increasing separation.

For an Au plate interacting with real graphene sheet the total thermal effect constitutes 21.5%, 34.4%, 53%, and 58% at $a = 100$, 200, 600, and 1000 nm, respectively [see the bottom solid line in Fig. 2 (left)]. From the bottom dashed line one finds 15.9%, 29.6%,53% and 58% for the implicit thermal correction to the Casimir pressure at $T = 0$ at the same respective separations. This means that for a real freesranding graphene sheet the role of explicit dependence of the polarization tensor on T as a parameter rapidly decreases with increasing separation.

Since in measurements of the Casimir force graphene is deposited on some substrate, we also illustrate its impact on the size of the thermal correction to the Casimir pressure. As a typical substrate, we consider a SiO_2 plate with a sufficiently accurate expression[57] for the dielectric permittivity $\varepsilon_l^{(2)}$. Now we perform computations of the thermal correction to the Casimir pressure between an Au plate and a real graphene sheet deposited on a SiO_2 plate by (2), (3)–(8) and (12). In $R_\lambda^{(1)}$ from (3) we again put $\Pi_{00,l} = \Pi_l = 0$ and use $\varepsilon_l^{(1)}$ for Au. In $R_\lambda^{(2)}$ we now use $\varepsilon_l^{(2)}$ for SiO_2 and the experimental values of Δ and μ indicated above for a real graphene sheet.

The computational results are shown in Fig. 2 (right) by the bottom solid line as a function of separation. The relative thermal correction is equal to 2.79%, 4.29%, 6.2%, and 6.2% of the Casimir pressure at $T = 0$ at $a = 100$, 200, 600, and 1000 nm, respectively. The bottom dashed line presents similar results for the implicit thermal correction to the Casimir pressure at $T = 0$. It is equal to 1.53%, 3.10%, 6.0%, and 6.2% at the same respective separations. For comparison purposes, in Fig. 2 (right) we also reproduce the bottom pair of solid and dashed lines from Fig. 2 (left) which shows the thermal corrections to the Casimir pressure between an Au plate and a freestanding real graphene sheet. In Fig. 2 (right) this pair takes the top position.

From Fig. 2 one can conclude that nonzero values of the energy gap and chemical potential of real graphene sample lead to a significant decrease of the thermal effect at short separations as compared to the case of a pristine graphene sheet. The thermal effect decreases further when the graphene sheet is deposited on a substrate

but still remains measurable in high precision experiments. Similar to the case of a freestanding graphene sample, for a graphene-coated substrate the role of an explicit contribution to the thermal effect rapidly decreases with increasing separation.

In the end of this section, we note that the thermal correction to the Casimir pressure from graphene depends heavily[48] on whether the condition $\Delta < 2\mu$ is satisfied (as in our case) or $\Delta > 2\mu$. Different aspects of the Casimir and Casimir-Polder interactions from graphene are investigated in a number of papers using the formalism of the polarization tensor.[58–71]

4. First Experiment on Measuring the Casimir Interaction from Graphene

In this experiment,[23] the gradient of the Casimir force was measured between an Au-coated hollow glass microsphere attached to an AFM cantilever and a graphene sheet deposited on a SiO_2 film covering a Si plate. The radius of the coated sphere was $R = 54.10 \pm 0.09$ μm and the thickness of an Au coating was 280 nm allowing to consider this sphere as all-gold. A large area graphene sample was obtained through a two-step chemical vapor deposition process.[72] The grown graphene sheet was transferred to a plate with $D = 300$ nm thick SiO_2 layer on top of a Si substrate of 500 μm thickness.

Measurements of the gradient of the Casimir force were performed at room temperature $T = 300$ K in high vacuum down to 10^{-9} Torr using the dynamic measurement scheme employed earlier in measuring the Casimir interaction between metallic surfaces.[73,74] The total force

$$F_{\rm tot}(a,T) = F_{\rm el}(a) + F_{sp}(a,T) \tag{13}$$

was the sum of an electric force $F_{\rm el}$ caused by the constant voltages V_i applied to graphene sheet while the sphere remained grounded and the Casimir force F_{sp} which depends on the temperature at the laboratory.

The force (13) leads to a modification of the resonant frequency of the cantilever-sphere system from ω_0 to some $\omega_r(a,T)$, and the frequency shift

$$\Delta\omega(a,T) = \omega_r(a,T) - \omega_0 \tag{14}$$

was measured by means of a phase-locked loop.

These measurements were performed at different separations in the linear regime of the oscillator where the frequency shift is connected with the gradient of the total force (13) according to[73,75]

$$\Delta\omega(a,T) = -CF'_{\rm tot}(a,T) = -CF'_{\rm el}(a) - CF'_{sp}(a,T). \tag{15}$$

The calibration constant C in (15) is given by $C = \omega_0/(2k)$ (k is the cantilever spring constant), $F'_{\rm el}$ is a known function[73] of the sphere radius, sphere-graphene separation $a = z_0 + z_{\rm piezo}$, where $z_{\rm piezo}$ is the distance moved by the graphene-coated SiO_2-Si substrate, z_0 is the closest sphere-graphene separation, and of the residual

potential difference V_0. Note that the values of z_0, V_0, and C are determined by means of electrostatic calibration. Then, the experimental values of the gradient of the Casimir force between an Au-coated sphere and a graphene-coated substrate are obtained from the measured frequency shift using (15)

$$F'_{sp}(a,T) = -\frac{1}{C}\Delta\omega(a,T) - F'_{\rm el}(a). \tag{16}$$

The comparison between experiment and theory was made by using the formalism presented in Sec. 2 and the proximity force approximation. In this approximation,[4,5] the Casimir force between a sphere and a plate is expressed as

$$F_{sp}(a,T) = 2\pi R\mathcal{F}(a,T), \tag{17}$$

where the Casimir free energy per unit area of two parallel plates is given by (1). By differentiating both sides of (17) with respect to a, one expresses the gradient of the Casimir force between a sphere and a graphene-coated substrate via the pressure between an Au plate and this substrate

$$F'_{sp}(a,T) = -2\pi RP(a,T). \tag{18}$$

The error introduced from using the approximate equality (18) has been shown as being less than a/R based on the exact theory of the Casimir force using the gradient expansion.[76–78] For the present experiment this error does not exceed 0.5% (see Sec. 5 for a more detailed information).

The theoretical force gradients should also be corrected for the presence of surface roughness.[4,5,79–81] In the framework of the multiplicative approach, which is sufficiently precise at short separations used in this experiment,[4,5] the gradient of the Casimir force corrected for the presence of roughness is given by

$$F'_{sp,{\rm theor}}(a,T) = \left(1 + 10\frac{\delta_s^2+\delta_g^2}{a^2}\right) F'_{sp}(a,T). \tag{19}$$

Here, the root-mean-square roughness amplitudes on the surfaces of the sphere and graphene measured by means of the usual AFM with a sharp tip are equal to $\delta_s = 1.6 \pm 0.1$ nm and $\delta_g = 1.5 \pm 0.1$ nm, respectively. Thus, the maximum contribution of the surface roughness is equal to only 0.1% at the shortest separation in this experiment.

Computations of the Casimir pressure in (18) were performed by (2) at $T = 300$ K as follows.[24] The reflection coefficients $R_\lambda^{(1)}$ on an Au surface are given by (3) where one should put $\Pi_{00,l} = \Pi_l = 0$ and use $\varepsilon_l^{(1)}$ for Au (see Sec. 3). The reflection coefficients $R_\lambda^{(2)}$ in (1) should be replaced with

$$\widetilde{R}_\lambda^{(2)}(i\xi_l,k_\perp) = \frac{R_\lambda^{(2)}(i\xi_l,k_\perp) + r_\lambda^{(2)}(i\xi_l,k_\perp)\,e^{-2Dk_l^{(2)}}}{1 + R_\lambda^{(2)}(i\xi_l,k_\perp)r_\lambda^{(2)}(i\xi_l,k_\perp)\,e^{-2Dk_l^{(2)}}} \tag{20}$$

because in this experiment graphene is deposited on a SiO_2 film of thickness D covering the Si plate.

Here, the coefficients $R_\lambda^{(2)}$ are defined in (3) where the permittivity $\varepsilon_l^{(2)}$ for SiO_2 was discussed in Sec. 3. The polarization tensor $\Pi_{00,l}$ and Π_l entering $R_\lambda^{(2)}$ is given in (5)–(8). It was used[24] with $\mu = 0$ and Δ varying from 0 to 0.1 eV (the exact values for the experimental graphene sample were not determined). As to the reflection coefficients $r_\lambda^{(2)}$ in (20), they describe the reflection on the boundary plane between semispaces made of SiO_2 and Si and have the standard form

$$r_{\rm TM}^{(2)}(i\xi_l,k_\perp)=\frac{\varepsilon_l^{\rm Si}k_l^{(2)}-\varepsilon_l^{(2)}k_l^{\rm Si}}{\varepsilon_l^{\rm Si}k_l^{(2)}+\varepsilon_l^{(2)}k_l^{\rm Si}}, \qquad r_{\rm TE}^{(2)}(i\xi_l,k_\perp)=\frac{k_l^{(2)}-\varepsilon_l^{(2)}k_l^{\rm Si}}{k_l^{(2)}+\varepsilon_l^{(2)}k_l^{\rm Si}}, \tag{21}$$

where $k_l^{\rm Si}=(k_\perp^2+\varepsilon_l^{\rm Si}\xi_l^2/c^2)^{1/2}$.

The dielectric permittivity of Si along the imaginary frequency axis, $\varepsilon_l^{\rm Si}=\varepsilon^{\rm Si}(i\xi_l)$, added some uncertainty in the theoretical analysis of this experiment. The B-doped Si plate used[23] had a nominal resistivity between 0.001 and 0.005 $\Omega\,$cm. This leads[82] to a density of charges varying from 1.6×10^{19} to 7.8×10^{19} cm^{-3} which is above the critical value 3.95×10^{18} cm^{-3} at which the dielectric-to-metal transition occurs.[83] The resulting plasma frequency ω_p varied in the relatively wide range[23] between 5×10^{14} and 11×10^{14} rad/s and was used in the extrapolation of the Si optical data[56] to zero frequency.

In Fig. 3, the measured gradients of the Casimir force from (16) between an Au-coated sphere and graphene-coated substrate are shown as crosses. The arms of the crosses indicate the total experimental errors in measuring the force gradients and separations determined at the 67% confidence level. The theoretical gradients of the Casimir force computed as a function of separation by (18) and (19), as explained above, are shown as the dark gray bands over the intervals from 224 to 280 nm (left) and from 280 to 350 nm (right). The width of the bands is mostly determined by the uncertainties in the values of ω_p for the Si plate and in the energy gap Δ of graphene.

Over the entire measurement range from 224 to 500 nm (Fig. 3 illustrates only a

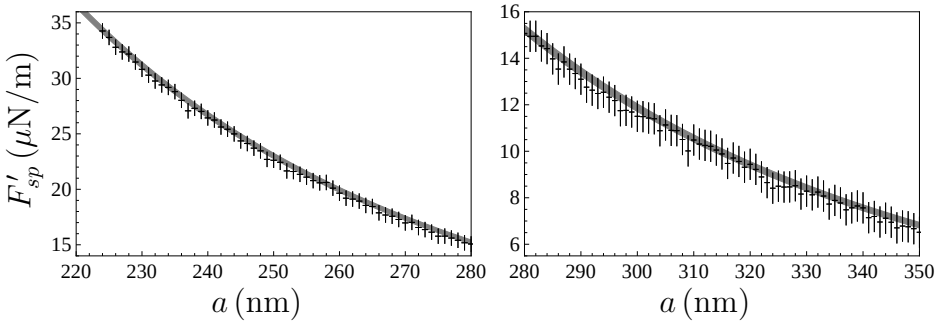


Fig. 3. The gradients of the Casimir force between an Au-coated sphere and a graphene sheet deposited on a SiO_2 film covering a Si plate computed at $T = 300$ K using the polarization tensor are shown as functions of separation by the dark gray band over the intervals from 224 to 280 nm (left) and from 280 to 350 nm (right). The measurement data are indicated as crosses.

part of this interval) the theoretical force gradients were found to be in good agreement with the predictions of the Lifshitz theory describing the electromagnetic response of graphene by means of the polarization tensor.[24] Note that theoretical predictions of the same theory using the reflection coefficients found in the framework of the hydrodynamic model of graphene are excluded by the measurement data of this experiment.[84] The question remains of what this experiment says about the large thermal effect in the Casimir force from graphene which, according to Sec. 3, should exist and be observable at short separations below 1 μm.

The question above was investigated[25] taking into account the experimental uncertainties and the material properties of the substrate supporting the graphene sheet. The gradient of the Casimir force at zero temperature was computed using the same formalism as above but replacing the summation in (2) with integration along the imaginary frequency axis in accordance with (11). The obtained computational results are shown in Fig. 4 by the bottom (light gray) band as a function of separation. The width of this band was found using the same uncertainties as considered above in computations of the Casimir force at $T = 300$ K. The theoretical band computed at $T = 300$ K is reproduced from Fig. 3 as the top (dark gray) band together with the measurement data indicated as the crosses. As can be seen in Fig. 4, the thickness of the bottom band computed at $T = 0$ K is somewhat larger than of the top one computed at $T = 300$ K. This is because under the condition $\Delta > 2\mu$ (later[48] the value of the chemical potential in this experiment was estimated as $\mu \approx 0.02$ eV) an impact of the nonzero energy gap Δ, which can be as much as 0.1 eV, on the force gradient is stronger at zero temperature.

From Fig. 4 it is seen that the bottom theoretical band computed at $T = 0$ K is slightly below the measurement data which, however, touch it in a number of data points. This suggests that there is some evidence in favor of the presence of thermal effect which, nevertheless, cannot be considered as a solid confirmation for

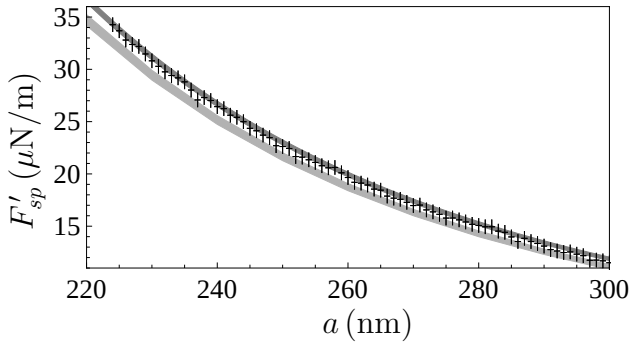


Fig. 4. The gradients of the Casimir force between an Au-coted sphere and a graphene sheet deposited on a SiO_2 film covering a Si plate computed at $T = 300$ K and $T = 0$ K using the polarization tensor are shown as functions of separation by the top (dark gray) and bottom (light gray) bands, respectively. The measurement data are indicated as crosses.

its existence.

According to the results obtained,[25] an impact of graphene deposited on a dielectric substrate on the thermal Casimir force increases with decreasing dielectric permittivity of the substrate material. This means that the SiO_2 substrate is appropriate for observation of the thermal effect in the Casimir force from graphene. It was concluded, however, that to attain this goal it is necessary to increase the thickness of the SiO_2 film up to at least 2 μm in order to eliminate the detrimental impact of the Si substrate. Following this analysis, it has become possible to demonstrate the large thermal effect in the next experiment on measuring the Casimir interaction from graphene.

5. Demonstration of Large Thermal Effect in the Casimir Interaction from Graphene

In the second experiment on measuring the Casimir interaction from graphene,[27,28] an Au-coated hollow glass microsphere of radius $R = 60.35 \pm 0.5$ μm was used as the first test body, whereas the second one was a graphene sheet deposited on top of thick SiO_2 substrate. Thus, the Si plate, which added uncertainty to the comparison between experiment and theory in the first experiment (see Sec. 4), was removed.

The graphene sheet used was made from a large-area graphene sample grown on a Cu foil using the method of chemical vapor deposition.[85] This sheet was transferred onto an optically polished SiO_2 substrate of 10 cm diameter and 0.05 cm thickness[86] using an electrochemical delamination procedure.[85,87]

An important new feature of the second experiment, as compared to the first one, is that a small but nonzero mass of electronic quasiparticles in graphene, which leads to an energy gap Δ in their spectrum,[15,16] was directly measured rather than estimated in some qualitative manner. This was made by means of scanning tunneling spectroscopy[88] and resulted in the value $\Delta = 0.29 \pm 0.05$ eV exceeding the one estimated in the first experiment.

Another important feature addressed in the second experiment is that any real graphene sheet contains some fraction of impurities and, as a result, is characterized by a nonzero value of the chemical potential.[15,16] The polarization tensor of graphene, taking the chemical potential of graphene μ into account, was derived[21] only in 2016. Because of this, in the course of first experiment it was not possible to reliably calculate the impact of impurities on the gradient of the Casimir force.

In the second experiment, the mean concentration of impurities in the graphene sheet was measured by Raman spectroscopy[89] with the result $\bar{n} = (4.2 \pm 0.3) \times 10^{12}$ cm^{-2}. Due to the transfer process used the expected dominant type of impurities was Na. Then the value of the chemical potential at $T = 0$ K was found[90]

$$\mu = \hbar v_{\rm F} \sqrt{\pi \bar{n}} = 0.24 \pm 0.01 \ \text{eV}. \tag{22}$$

This value can also be used at room temperature because the relatively large chemical potential $\mu = 0.24$ eV is almost temperature-independent.[91]

The measurement scheme of the gradient of the Casimir force was the same as in the first experiment described in Sec. 4. This means that measurements were performed in high vacuum at $T = 294.0 \pm 0.5$ K temperature by using a modified AFM cantilever-based technique operated in the dynamic mode. There was, however, an important improvement allowing a significant decrease of the total experimental error in measuring the force gradient. The AFM cantilever spring constant k was reduced through chemical etching (like it was done in a recent experiment with metallic test bodies[10]) leading to the corresponding decrease of the resonant frequency of the cantilever ω_0. As a result, the value of the calibration constant C in (16) was increased by up to a factor 8 leading to a significant decrease of the total experimental error from 0.64 μN/m in the first experiment (see Fig. 3) to 0.14 μN/m in the second.

Computations of the gradients of the Casimir force were performed by (2) using the reflection coefficients (3), the polarization tensor (5)–(8), and the equalities (18) and (19). In the reflection coefficients $R_\lambda^{(1)}$ one should put $\Pi_{00,l} = \Pi_l = 0$ and take for $\varepsilon_l^{(1)}$ the values of the dielectric permittivity of Au at pure imaginary Matsubara frequencies. In $R_\lambda^{(2)}$ the polarization tensor at $T = 294$ K is taken with $\Delta = 0.29$ eV and $\mu = 0.24$ eV as was measured for a graphene sheet used and the dielectric permittivity $\varepsilon_l^{(2)}$ refers to a SiO_2 substrate. The root-mean-square roughness amplitudes on the surfaces of a sphere and graphene were measured to be $\delta_s = 0.9 \pm 0.1$ nm and $\delta_g = 1.5 \pm 0.1$ nm, respectively.

The computational results for the gradient of the Casimir force are shown in Fig. 5 as the functions of separation by the top (dark gray) bands over the intervals from 250 to 300 nm (left) and from 300 to 400 nm (right). The width of these bands is determined in the following conservative way. The upper boundary lines of the theoretical bands were computed with the largest allowed value of $\mu = 0.25$ eV and the smallest allowed value of $\Delta = 0.24$ eV. The lower boundary lines were computed

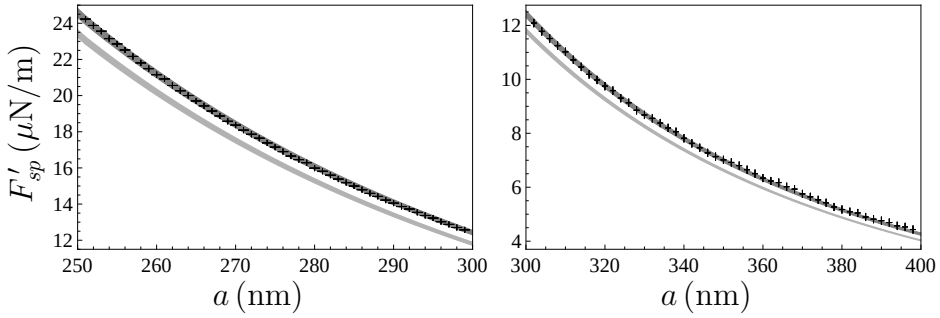


Fig. 5. The gradients of the Casimir force between an Au-coted sphere and a graphene sheet deposited on a SiO_2 substrate computed at $T = 294$ K and $T = 0$ K are shown as functions of separation by the top (dark gray) and bottom (light gray) bands, respectively, over the intervals from 250 to 300 nm (left) and from 300 to 400 nm (right). The measurement data are indicated as crosses.

with the smallest allowed value of $\mu = 0.23$ eV and the largest allowed value of $\Delta = 0.34$ eV. This is because an increase of μ with fixed Δ increases the force gradient, whereas an increase of Δ with $\mu = \text{const}$ decreases the force gradient.[48] The width of the theoretical band was also increased to take into account the 0.5% errors arising from uncertainties in the optical data of Au and SiO_2 and the error in the sphere radius indicated above.

As was mentioned in Sec. 4, the theoretical force gradients computed by (18) are burdened with an error due to the deviations from PFA. According to the results obtained using the gradient expansion[76–78,92] and the scattering approach,[93–96] in the sphere-plate geometry the PFA leads to slightly larger force gradients than are given by the exact computations using these methods. Because of this, the upper boundary lines of the top theoretical bands in Fig. 5 remained as they are with no correction for the PFA error. As to the lower lines bounding the theoretical bands, they are corrected for a maximum possible correction factor of $(1 - a/R)$.

The experimental gradients of the Casimir force are shown in Fig. 5 as the crosses whose arms indicate the total experimental errors determined at the 67% confidence level. It is seen that the measurement data are in good agreement with theoretical predictions of the top band computed using the polarization tensor at $T = 294$ K with the measured values of Δ and μ. Similar good agreement holds[27,28] in the remaining range of experimental separations from 400 to 700 nm which is not shown in Fig. 5.

The computations of the gradient of the Casimir force were repeated at $T = 0$ K. In so doing, a summation in the Matsubara frequencies in (2) was replaced with an integration over continuous ξ in accordance to (11). It is important to stress that for a real graphene sheet with $\Delta < 2\mu$ (as in this experiment) the polarization tensor at $T = 0$ K is not given by (6) but is defined by the equalities

$$\Pi_{00}(i\xi, k_\perp, 0, \Delta, \mu) = \Pi_{00}^{(0)}(i\xi, k_\perp, \Delta) + \lim_{T\to 0}\Pi_{00}^{(1)}(i\xi, k_\perp, T, \Delta, \mu),$$
$$\Pi(i\xi, k_\perp, 0, \Delta, \mu) = \Pi^{(0)}(i\xi, k_\perp, \Delta) + \lim_{T\to 0}\Pi^{(1)}(i\xi, k_\perp, T, \Delta, \mu). \qquad (23)$$

As a result, Π_{00} and Π at $T = 0$ K depend both on Δ and μ in this case [under the condition $\Delta > 2\mu$ the polarization tensor at $T = 0$ K is given[48] by (6) and, thus, does not depend on μ].

The computational results for the gradient of the Casimir force at $T = 0$ K are shown in Fig. 5 as the functions of separation by the bottom (light gray) bands over the intervals from 250 to 300 nm (left) and from 300 to 400 nm (right). The thickness of these bands is computed in the same conservative way as the top ones taking into account all theoretical uncertainties and errors as explained above. According to Fig. 5, the top bands do not intersect with the bottom ones demonstrating the predicted large thermal effect from graphene at short separations. The same holds[27,28] at separations up to $a = 517$ nm (at larger separations both bands overlap). Thus, this experiment demonstrates the presence of the thermal effect in the gradient of the Casimir force from graphene sample in the region of relatively

short separations from 250 to 517 nm.

To explicitly demonstrate the observed thermal effect, in Fig. 6 we show the thermal correction to the gradient of the Casimir force equal to a difference between the mean measured gradients presented in Fig. 5 and the theoretical ones computed at $T = 0$ K as a function of separation. This correction constitutes 4%, 5%, 7%, and 8.5% of the total gradient of the Casimir force at separations $a = 250$, 300, 400, and 500 nm, respectively. As is seen in Fig. 6, its absolute values are significantly larger than the total error in measuring the gradient of the Casimir force equal to 0.14 μN/m.

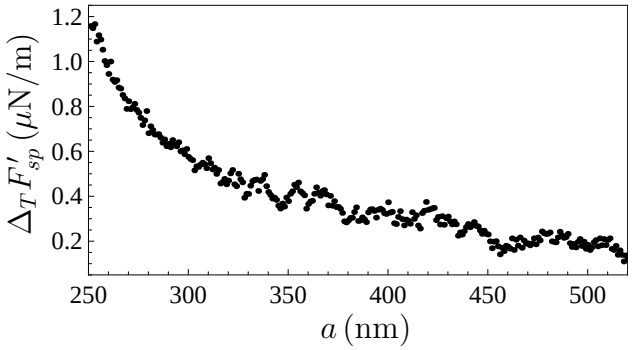


Fig. 6. The observed thermal correction to the gradient of the Casimir force between an Au-coated sphere and a graphene-coated SiO_2 substrate is shown as a function of separation.

6. Conclusions and Discussion

In the foregoing, we have considered the Casimir effect from graphene. This is a novel material which has already demonstrated several unusual features of its mechanical, electrical, and optical properties. As mentioned in Sec. 1, the striking feature of the Casimir effect between two pristine graphene sheets is a predicted[26] huge thermal correction equal to thousands of percent of the zero-temperature pressure even at short separations of a few hundred nanometers. This effect should be compared with a few percent thermal correction to the Casimir pressure between two parallel metallic plates described by the Drude model which was excluded by the results of many high precision experiments.

As discussed in Sec. 2, the Casimir effect from graphene at separations exceeding 100 nm can be reliably described by using the Lifshitz theory where the dielectric response of graphene is expressed via the polarization tensor at nonzero temperature accounting for the nonzero energy gap and chemical potential. Taking into consideration that the explicit expression for the polarization tensor is derived from the first principles of quantum electrodynamics at nonzero temperature and provides the correct description of the electrical and optical properties of graphene,[97,98]

the crucial question arises whether the predicted huge thermal effect does occur in nature.

In Sec. 3, it is shown that for real graphene sheets possessing nonzero energy gap and chemical potential the predicted effect is significantly suppressed. In the case of graphene-coated dielectric substrate interacting with a metallic plate at separations of a few hundred nanometers, its size is reduced to a few percent, i.e., to the same value as an experimentally excluded thermal correction for metals described by the Drude model. At the same time, the Lifshitz theory using the dielectric response of graphene given by the polarization tensor was found to be in agreement with the Nernst heat theorem which is not the case for an idealized model of Drude metals with perfect crystal lattices and for dielectric materials described by the frequency-dependent dielectric permittivity with inclusion of the conductivity at nonzero temperature. This adds considerable significance to the experimental investigation of the Casimir effect from graphene.

The first experiment on measuring the Casimir interaction from graphene,[23] considered in Sec. 4, was found[24] in good agreement with theoretical predictions of the Lifshitz theory using the polarization tensor. Taking into account the relatively large experimental and theoretical errors from the not fully characterized graphene sample and the two-layer substrate, and the unavailability of the polarization tensor accounting for the chemical potential at that time, it was not possible to reliably separate only a few percent thermal effect from the total measured force gradient.

These problems were successfully solved in the second, refined, experiment on measuring the gradient of the Casimir force between an Au-coated sphere and a graphene-coated SiO_2 substrate discussed in Sec. 5. In this experiment,[27,28] the single-layer thick dielectric substrate has been used made of a material with low static dielectric permittivity which is favorable for an observation of the thermal effect.[25] What is more, the graphene sheet was carefully characterized by performing independent measurements of its energy gap and chemical potential. By reducing the spring constant of the AFM cantilever through chemical etching, the calibration constant of the oscillator was increased by up to a factor of 8. In the end, the total experimental error in the second experiment was reduced by the factor of 4.6 as compared to the first one.

Finally, the theoretical gradients of the Casimir force in the experimental configuration have been computed using the Lifshitz theory and the exact polarization tensor of graphene taking into account the nonzero values of its energy gap and chemical potential. The theoretical values at the experimental temperature $T = 294$ K were found in good agreement with the measurement data over the entire range of separations from 250 to 700 nm with no fitting parameters. The comparison of the same data with the theoretical force gradients computed at $T = 0$ K unambiguously demonstrated the presence of the predicted thermal effect which size ranges from 4% to 8.5% of the total force gradient when separation increases from 250 to 500 nm, respectively.

Thus, the Lifshitz theory using the exact response functions of graphene to

electromagnetic fluctuations does not have any problems being in good agreement with both the measurement data and with the principles of thermodynamics. The long-term problems in theoretical description of the Casimir force between metallic surfaces mentioned in Sec. 1 arise when a metal is described by the Drude model which has been carefully tested in the area of propagating waves. Because of this, one may suggest that this phenomenological model fails to provide an adequate description of the electromagnetic response to evanescent waves which are off the mass shell in the free space but make an important contribution to the Casimir force. Taking into account that the polarization tensor of graphene is equivalent to the spatially nonlocal dielectric permittivities, the Drude-like phenomenological nonlocal response functions were proposed[99–102] which nearly coincide with the Drude model in the area of propagating waves but bring the Lifshitz theory in agreement with both thermodynamics and experiment for the test bodies made of nonmagnetic and magnetic metals.

Hence, the fundamental description of an electromagnetic response in the case of 3D material bodies (an attempt in this direction was undertaken recently[103]), as has been made for graphene, may be also helpful in solving the complicated problems of Casimir physics for usual materials.

Acknowledgments

The work of U. M. was partially supported by the NSF grant PHY-2012201. The work of G. L. K. and V. M. M. was partially supported by the Peter the Great Saint Petersburg Polytechnic University in the framework of the Russian state assignment for basic research (project No. FSEG-2020-0024). This paper has been supported by the Kazan Federal University Strategic Academic Leadership Program.

References

1. H. B. G. Casimir, *Proc. Kon. Ned. Akad. Wet. B* **51**, 793 (1948).
2. E. M. Lifshitz, *Zh. Eksp. Teor. Fiz.* **29**, 94 (1955) [*Sov. Phys. JETP* **2**, 73 (1956)].
3. E. M. Lifshitz and L. P. Pitaevskii, *Statistical Physics, Part II* (Pergamon, Oxford, 1980).
4. G. L. Klimchitskaya, U. Mohideen and V. M. Mostepanenko, *Rev. Mod. Phys.* **81**, 1827 (2009).
5. M. Bordag, G. L. Klimchitskaya, U. Mohideen and V. M. Mostepanenko, *Advances in the Casimir Effect* (Oxford University Press, Oxford, 2015).
6. L. M. Woods, D. A. R. Dalvit, A. Tkatchenko, P. Rodriguez-Lopez, A. W. Rodriguez and R. Podgornik, *Rev. Mod. Phys.* **88**, 045003 (2016).
7. V. M. Mostepanenko, *Universe* **7**, 84 (2021).
8. G. Bimonte, D. López and R. S. Decca, *Phys. Rev. B* **93**, 184434 (2016).
9. M. Liu, J. Xu, G. L. Klimchitskaya, V. M. Mostepanenko and U. Mohideen, *Phys. Rev. B* **100**, 081406(R) (2019).
10. M. Liu, J. Xu, G. L. Klimchitskaya, V. M. Mostepanenko and U. Mohideen, *Phys. Rev. A* **100**, 052511 (2019).
11. G. Bimonte, B. Spreng, P. A. Maia Neto, G.-L. Ingold, G. L. Klimchitskaya, V. M. Mostepanenko and R. S. Decca, *Universe* **7**, 93 (2021).

12. A. H. Castro Neto, F. Guinea, N. M. R. Peres, K. S. Novoselov and A. K. Geim, *Rev. Mod. Phys.* **81**, 109 (2009).
13. N. M. R. Peres, *Rev. Mod. Phys.* **82**, 2673 (2010).
14. S. Das Sarma, S. Adam, E. H. Hwang and E. Rossi, *Rev. Mod. Phys.* **83**, 407 (2011).
15. H. Aoki and M. S. Dresselhaus (eds.), *Physics of Graphene* (Springer, Cham, 2014).
16. M. I. Katsnelson, *The Physics of Graphene* (Cambridge University Press, Cambridge, 2020).
17. T. Zhu, M. Antezza and J.-S. Wang, *Phys. Rev. B* **103**, 125421 (2021).
18. M. Bordag, I. V. Fialkovsky, D. M. Gitman and D. V. Vassilevich, *Phys. Rev. B* **80**, 245406 (2009).
19. I. V. Fialkovsky, V. N. Marachevsky and D. V. Vassilevich, *Phys. Rev. B* **84**, 035446 (2011).
20. M. Bordag, G. L. Klimchitskaya, V. M. Mostepanenko and V. M. Petrov, *Phys. Rev. D* **91**, 045037 (2015) [Erratum: *ibid.* **93**, 089907 (2016)].
21. M. Bordag, I. Fialkovskiy and D. Vassilevich, *Phys. Rev. B* **93**, 075414 (2016) [Erratum: *ibid.* **95**, 119905 (2017)].
22. M. Dressel and G. Grüner, *Electrodynamics of Solids: Optical Properties of Electrons in Metals* (Cambridge University Press, Cambridge, 2003).
23. A. A. Banishev, H. Wen, J. Xu, R. K. Kawakami, G. L. Klimchitskaya, V. M. Mostepanenko and U. Mohideen, *Phys. Rev. B* **87**, 205433 (2013).
24. G. L. Klimchitskaya, U. Mohideen and V. M. Mostepanenko, *Phys. Rev. B* **89**, 115419 (2014).
25. G. L. Klimchitskaya and V. M. Mostepanenko, *Phys. Rev. A* **89**, 052512 (2014).
26. G. Gómez-Santos, *Phys. Rev. B* **80**, 245424 (2009).
27. M. Liu, Y. Zhang, G. L. Klimchitskaya, V. M. Mostepanenko and U. Mohideen, *Phys. Rev. Lett.* **126**, 206802 (2021).
28. M. Liu, Y. Zhang, G. L. Klimchitskaya, V. M. Mostepanenko and U. Mohideen, *Phys. Rev. B* **104**, 085436 (2021).
29. O. Kenneth and I. Klich, *Phys. Rev. B* **78**, 014103 (2008).
30. T. Emig, N. Graham, R. L. Jaffe and M. Kardar, *Phys. Rev. D* **77**, 025005 (2008).
31. S. J. Rahi, T. Emig, N. Graham, R. L. Jaffe and M. Kardar, *Phys. Rev. D* **80**, 085021 (2009).
32. G. Barton, *J. Phys. A: Math. Gen.* **38**, 2997 (2005).
33. M. Bordag, *J. Phys. A: Math. Gen.* **39**, 6173 (2006).
34. M. Bordag, B. Geyer, G. L. Klimchitskaya and V. M. Mostepanenko, *Phys. Rev. B* **74**, 205431 (2006).
35. L. A. Falkovsky and A. A. Varlamov, *Eur. Phys. J. B* **56**, 281 (2007).
36. L. A. Falkovsky and S. S. Pershoguba, *Phys. Rev. B* **76**, 153410 (2007).
37. D. Drosdoff, A. D. Phan, L. M. Woods, I. V. Bondarev and J. F. Dobson, *Eur. Phys. J. B* **85**, 365 (2012).
38. J. F. Dobson, A. White and A. Rubio, *Phys. Rev. Lett.* **96**, 073201 (2006).
39. T. Stauber, N. M. R. Peres and A. K. Geim, *Phys. Rev. B* **78**, 085432 (2008).
40. Bo E. Sernelius, *Europhys. Lett.* **95**, 57003 (2011).
41. J. Sarabadani, A. Naji, R. Asgari and R. Podgornik, *Phys. Rev. B* **84**, 155407 (2011); *Phys. Rev. B* **87**, 239905(E) (2013).
42. Bo E. Sernelius, *Phys. Rev. B* **85**, 195427 (2012); **89**, 079901(E) (2014).
43. C. Abbas, B. Guizal and M. Antezza, *Phys. Rev. Lett.* **118**, 126101 (2017).
44. D. Drosdoff and L. M. Woods, *Phys. Rev. B* **82**, 155459 (2010).
45. D. Drosdoff and L. M. Woods, *Phys. Rev. A* **84**, 062501 (2011).
46. A. D. Phan, N. A. Viet, N. A. Poklonski, L. M. Woods and C. H. Le, *Phys. Rev. B*

86, 155419 (2012).
47. G. L. Klimchitskaya and V. M. Mostepanenko, *Phys. Rev. B* **91**, 174501 (2015).
48. G. Bimonte, G. L. Klimchitskaya and V. M. Mostepanenko, *Phys. Rev. B* **96**, 115430 (2017).
49. G. L. Klimchitskaya, V. M. Mostepanenko and Bo E. Sernelius, *Phys. Rev. B* **89**, 125407 (2014).
50. V. B. Bezerra, G. L. Klimchitskaya, V. M. Mostepanenko and C. Romero, *Phys. Rev. A* **94**, 042501 (2016).
51. G. L. Klimchitskaya and V. M. Mostepanenko, *Phys. Rev. D* **102**, 016006 (2020).
52. G. L. Klimchitskaya and V. M. Mostepanenko, *Phys. Rev. A* **98**, 032506 (2018).
53. G. L. Klimchitskaya and V. M. Mostepanenko, *Phys. Rev. D* **101**, 116003 (2020).
54. G. L. Klimchitskaya and V. M. Mostepanenko, *Universe* **6**, 150 (2020).
55. G. L. Klimchitskaya and V. M. Mostepanenko, *Phys. Rev. B* **87**, 075439 (2013).
56. E. D. Palik (ed.), *Handbook of Optical Constants of Solids* (Academic Press, New York, 1985).
57. L. Bergström, *Adv. Colloid Interface Sci.* **70**, 125 (1997).
58. M. Bordag, G. L. Klimchitskaya and V. M. Mostepanenko, *Phys. Rev. B* **86**, 165429 (2012).
59. M. Chaichian, G. L. Klimchitskaya, V. M. Mostepanenko and A. Tureanu, *Phys. Rev. A* **86**, 012515 (2012).
60. B. Arora, H. Kaur and B. K. Sahoo, *J. Phys. B* **47**, 155002 (2014).
61. K. Kaur, J. Kaur, B. Arora and B. K. Sahoo, *Phys. Rev. B* **90**, 245405 (2014).
62. G. L. Klimchitskaya and V. M. Mostepanenko, *Phys. Rev. A* **89**, 012516 (2014).
63. G. L. Klimchitskaya and V. M. Mostepanenko, *Phys. Rev. B* **89**, 035407 (2014).
64. G. L. Klimchitskaya and V. M. Mostepanenko, *Phys. Rev. A* **89**, 062508 (2014).
65. G. L. Klimchitskaya, *Int. J. Mod. Phys. A* **31**, 1641026 (2016).
66. G. Bimonte, G. L. Klimchitskaya and V. M. Mostepanenko, *Phys. Rev. A* **96**, 012517 (2017).
67. M. Bordag, I. Fialkovsky, D. Vassilevich, *Phys. Lett. A* **381**, 2439 (2017).
68. C. Henkel, G. L. Klimchitskaya and V. M. Mostepanenko, *Phys. Rev. A* **97**, 032504 (2018).
69. N. Khusnutdinov and N. Emelianova, *Int. J. Mod. Phys. A* **34**, 1950008 (2019).
70. N. Khusnutdinov and N. Emelianova, *Universe* **7**, 70 (2021).
71. G. L. Klimchitskaya, *Mod. Phys. Lett. A* **35**, 2040004 (2020).
72. X. Li, C. W. Magnuson, A. Venugopal, R. M. Tromp, J. B. Hannon, E. M. Vogel, L. Colombo and R. S. Ruoff, *J. Am. Chem. Soc.* **133**, 2816 (2011).
73. C.-C. Chang, A. A. Banishev, R. Castillo-Garza, G. L. Klimchitskaya, V. M. Mostepanenko and U. Mohideen, *Phys. Rev. B* **85**, 165443 (2012).
74. A. A. Banishev, C.-C. Chang, G. L. Klimchitskaya, V. M. Mostepanenko and U. Mohideen, *Phys. Rev. B* **85**, 195422 (2012)
75. F. J. Giessibl, *Rev. Mod. Phys.* **75**, 949 (2003).
76. C. D. Fosco, F. C. Lombardo and F. D. Mazzitelli, *Phys. Rev. D* **84**, 105031 (2011).
77. G. Bimonte, T. Emig, R. L. Jaffe and M. Kardar, *Europhys. Lett.* **97**, 50001 (2012).
78. G. Bimonte, T. Emig and M. Kardar, *Appl. Phys. Lett.* **100**, 074110 (2012).
79. M. Bordag, G. L. Klimchitskaya and V. M. Mostepanenko, *Int. J. Mod. Phys. A* **10**, 2661 (1995).
80. P. J. van Zwol, G. Palasantzas and J. Th. M. De Hosson, *Phys. Rev. B* **77**, 075412 (2008).
81. W. Broer, G. Palasantzas, J. Knoester and V. B. Svetovoy, *Phys. Rev. B* **85**, 155410 (2012).

82. W. E. Beadle, J. C. C. Tsai and R. D. Plummer (eds.), *Quick Reference Manual for Silicon Integrated Circuit Technology* (Wiley, New York, 1985).
83. P. Dai, Y. Zhang and M. P. Sarachik, *Phys. Rev. Lett.* **66**, 1914 (1991).
84. G. L. Klimchitskaya and V. M. Mostepanenko, *Phys. Rev. B* **91**, 045412 (2015).
85. Grolltex, San Diego, CA, http://www.grolltex.com
86. MSE Supplies, Tucson, AZ, http://www.msesupplies.com
87. Y. Wang, Y. Zheng, X. Xu, E. Dubuisson, Q. Bao, J. Lu and K. Ping Loh, *ACS Nano* **5**, 9927 (2011).
88. G. Li, A. Luican and E. Y. Andrei, *Phys. Rev. Lett.* **102**, 176804 (2009).
89. A. Das, S. Pisana, B. Chakraborty, S. Piscanec, S. K. Saha, U. V. Waghmare, K. S. Novoselov, H. R. Krishnamurthy, A. K. Geim, A. C. Ferrari and A. K. Sood, *Nature Nanotech.* **3**, 210 (2008).
90. L. A. Falkovsky, *J. Phys.: Conf. Series* **129**, 012004 (2008).
91. L. A. Falkovsky, *Pis'ma v ZETF* **98**, 183 (2013) [*JETP Letters* **98**, 161 (2013)].
92. G. Bimonte, *Europhys. Lett.* **118**, 20002 (2017).
93. M. Hartmann, G.-L. Ingold and P. A. Maia Neto, *Phys. Rev. Lett.* **119**, 043901 (2017).
94. B. Spreng, M. Hartmann, V. Henning, P. A. Maia Neto and G.-L. Ingold, *Phys. Rev. A* **97**, 062504 (2018).
95. M. Hartmann, G.-L. Ingold and P. A. Maia Neto, *Phys. Scr.* **93**, 114003 (2018).
96. V. Henning, B. Spreng, M. Hartmann, G.-L. Ingold and P. A. Maia Neto, *J. Opt. Soc. Amer. B* **36**, C77 (2019).
97. G. L. Klimchitskaya, V. M. Mostepanenko and V. M. Petrov, *Phys. Rev. B* **96**, 235432 (2017).
98. G. L. Klimchitskaya, V. M. Mostepanenko and V. M. Petrov, *Phys. Rev. A* **98**, 023809 (2018).
99. G. L. Klimchitskaya and V. M. Mostepanenko, *Eur. Phys. J. C* **80**, 900 (2020).
100. G. L. Klimchitskaya and V. M. Mostepanenko, *Phys. Rev. D* **103**, 096007 (2021).
101. G. L. Klimchitskaya and V. M. Mostepanenko, *Phys. Rev. D* **104**, 085001 (2021).
102. G. L. Klimchitskaya and V. M. Mostepanenko, *Phys. Rev. A* **105**, 012805 (2022).
103. M. Bordag, I. V. Fialkovsky, N. Khusnutdinov and D. V. Vassilevich, *Phys. Rev. B* **104**, 195431 (2021).